Chromene-based Schiff Base Ligand: DNA Interaction Studies and Characterization of Tetranuclear Zinc, Nickel and Iron Complexes

Andrew J. Ressler[a], Olivia N. Brandt[a], Ashton Weaver[a], Jenna E. Poor,[a] Anna Ream[a], Nicolas A. Summers[a], Colin D. McMillen[b], Navindra P. Seeram[c], William G. Dougherty[a*], Geneive E. Henry[a*]

[a]*Department of Chemistry, Susquehanna University, 514 University Avenue, Selinsgrove, PA 17870, USA*

[b]*Department of Chemistry, Clemson University, Clemson, SC 29634, USA*

[c]*Bioactive Botanical Research Laboratory*, *Department of Biomedical and Pharmaceutical Sciences, College of Pharmacy, University of Rhode Island, Kingston, RI 02881, USA*

***Corresponding authors:**

William G. Dougherty

Department of Chemistry, Susquehanna University, 514 University Avenue, Selinsgrove, PA 17870

Telephone: 570-372-4255

E-mail: doughertyw@susqu.edu

Geneive E. Henry

Department of Chemistry, Susquehanna University, 514 University Avenue, Selinsgrove, PA 17870

Telephone: 570-372-4222

E-mail: henry@susqu.edu

Abstract

Three Zn(II), Ni(II) and Fe(III) tetranuclear clusters have been prepared using a new chromene-based Schiff base ligand (H_2L) derived from the condensation of 2-aminophenol and 5-hydroxy-2,2-dimethyl-2H-chromene-6-carbaldehyde. The structures of the tetranuclear clusters were determined by single crystal X-ray diffraction and mass spectrometric analyses. The crystallographic data indicates that the Zn and Ni clusters have similar structures $[M_4L_4(THF)_2]$ and contain a defective dicubane core, with each ligand coordinated to one metal ion through three donor atoms. The iron complex was obtained as a tetranuclear star shaped cluster $[Fe_4L_6]$, consisting of a central Fe(III) ion coordinated to six oxygen atoms, with three Fe(III) ions forming the corners of an equilateral triangle. The metal-mediated DNA cleavage ability of the free ligand, H_2L, was determined using pBR322 plasmid DNA in the presence of Fe, Co, Ni, Cu, Zn and Cd acetate salts. H_2L in combination with the Cu(II) salt resulted in significant DNA cleavage. The interaction of the ligand with DNA was investigated by UV-Vis titrations and molecular docking studies, which indicated favorable docking in the minor groove of DNA.

Keywords: Chromene-based Schiff base; tetranuclear zinc, nickel and iron complexes; DNA cleavage; CT-DNA binding; molecular docking

Introduction

Metal complexes of Schiff base ligands are attractive candidates as pharmaceutical agents due to their ease of preparation, wide structural diversity, and range of biological properties.[1-2] For example, mononuclear, tridentate Schiff base complexes have been found to possess anticancer, antioxidant, antiviral, and antibacterial properties, as well as DNA binding activity.[3-9] These complexes have also been applied as catalysts for organic reactions.[10] Similar ligands have been applied to the synthesis of multinuclear clusters, which may have different properties than their mononuclear counterparts.[11-12] The structure of a given multinuclear cluster is often difficult to predict, being influenced by reaction stoichiometry, counterion identity, solvent, and other factors.[12-13]

Multinuclear transition metal clusters form a variety of interesting shapes, including defective dicubane and star-shaped complexes. The defective dicubane motif describes a tetranuclear cluster arranged in the form of two cubanes, stacked face-to-face, where each cube is missing one corner.[14] These structures are being explored as catalysts, materials, and molecular magnets.[15-19] Star-shaped tetranuclear complexes derived from ONO ligands contain a central metal ion coordinated to six oxygen atoms. The remaining three metal ions are each coordinated to two oxygen atoms and are at the corners of an equilateral triangle.[20-23] Like defective dicubanes, they have found applications as molecular magnets.[23-24]

In this study, we report the synthesis of a new chromene-based ONO donor Schiff base ligand, (*E*)-6-(((2-hydroxyphenyl)imino)methyl)-2,2-dimethyl-2*H*-chromen-5-ol (H_2L), and its use in the preparation of tetranuclear defective dicubane Zn(II) and Ni(II) complexes, as well as a tetranuclear star-shaped Fe(III) cluster. The DNA cleavage properties of the free ligand in the presence of acetate salts of iron, cobalt, nickel, copper, zinc and cadmium were also examined.

Finally, DNA binding was studied using both UV-Vis titrations and molecular docking simulations.

2 Results and Discussion

2.1 Synthesis of ligands and metal complexes

Chromene derivative (**1**) was synthesized using a published method.[25] Ligand H_2L was prepared by acid-catalyzed condensation of **1** with 2-aminophenol. Complexes **3-5** were prepared by the reaction of equimolar amounts of H_2L with the corresponding metal acetate salts, followed by crystal growth by the diffusion method (Scheme 1).

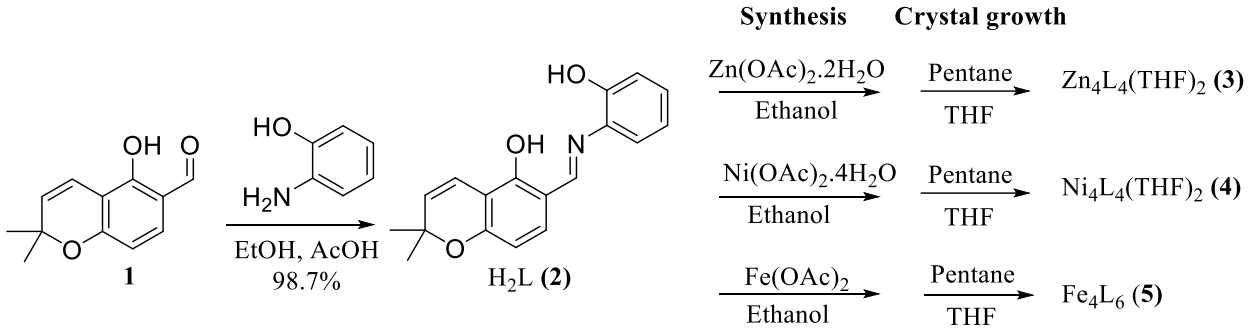

Scheme 1: Synthesis of metal complexes **3-5** from tridentate ONO ligand, H_2L (**2**).

2.2 Single Crystal X-ray Characterization of Complexes 3-5

Single crystals of the Zn(II), Ni(II) and Fe(III) complexes (**3-5**) were obtained by vapor diffusion of pentane into a saturated THF solution of the complex. Structure refinement parameters for the crystals are shown in Table 1. Interestingly, ligand H_2L appeared to favor the formation of multinuclear clusters in all cases where X-ray-quality crystals could be obtained.

Table 1. Crystallographic data and structure refinement parameters for **3-5**.

	$Zn_4L_4(THF)_2$ (3)	**$Ni_4L_4(THF)_2$ (4)**	**Fe_4L_6 (5)**
Chemical formula	$C_{80}H_{76}N_4O_{14}Zn_4$	$C_{80}H_{76}N_4Ni_4O_{14}$	$C_{120}H_{114}Fe_4N_6O_{21}$
Formula weight (g/mol)	1578.92	1552.28	2199.57
T (K)	150(2)	100(2)	100(2)
Crystal size (mm)	0.035 x 0.038 x 0.187	0.084 x 0.142 x 0.187	0.056 x 0.072 x 0.147
Crystal system	monoclinic	triclinic	monoclinic
Space group	*P*2(1)	*P*-1	*C*2/c
a (Å)	11.2925(8)	10.9075(4)	28.036(2)
b (Å)	31.975(2)	17.7587(6)	24.904(2)
c (Å)	11.4522(8)	19.3381(7)	15.356(2)
α (°)	90	68.096(2)	90
β (°)	119.368(2)	86.112(2)	99.766(3)°
γ (°)	90	84.897(2)	90
V ($Å^3$)	3603.7(4)	3459.2(2)	10566(2)
Z(Z')	2(1)	2(1)	4(0.5)
$_{calc}$ (g/cm^3)	1.455	1.490	1.383
μ (mm^{-1})	1.384	1.144	0.614
θ Range (°)	3.62 to 26.50	2.15 to 25.50	2.12 to 25.50
Goodness-of-fit on F^2	1.031	1.165	1.055
R(F), R_w(F); I > 2σ	0.0345, 0.0655	0.0515, 0.1007	0.0685, 0.1299

*2.2.1 Structure of $Zn_4L_4(THF)_2$, **3***

X-ray diffraction analysis of complex **3** revealed the formation of a defective dicubane tetranuclear Zn cluster, consisting of four Zn(II) ions, four L^{2-} ligands, and two coordinated THF molecules (Fig. 1). Each chromene-aminophenol ligand binds to one Zn center as a tridentate, ONO pincer-type ligand. Two ligands use their chromene phenolic oxygen atoms (O1, O7) to bind exclusively to their respective metal center, while the aminophenolate oxygen atoms of these ligands act as μ_3 bridging oxygen atoms (O3, O9). In the other two ligands, both the chomene and aminophenolate oxygen atoms are μ_2.

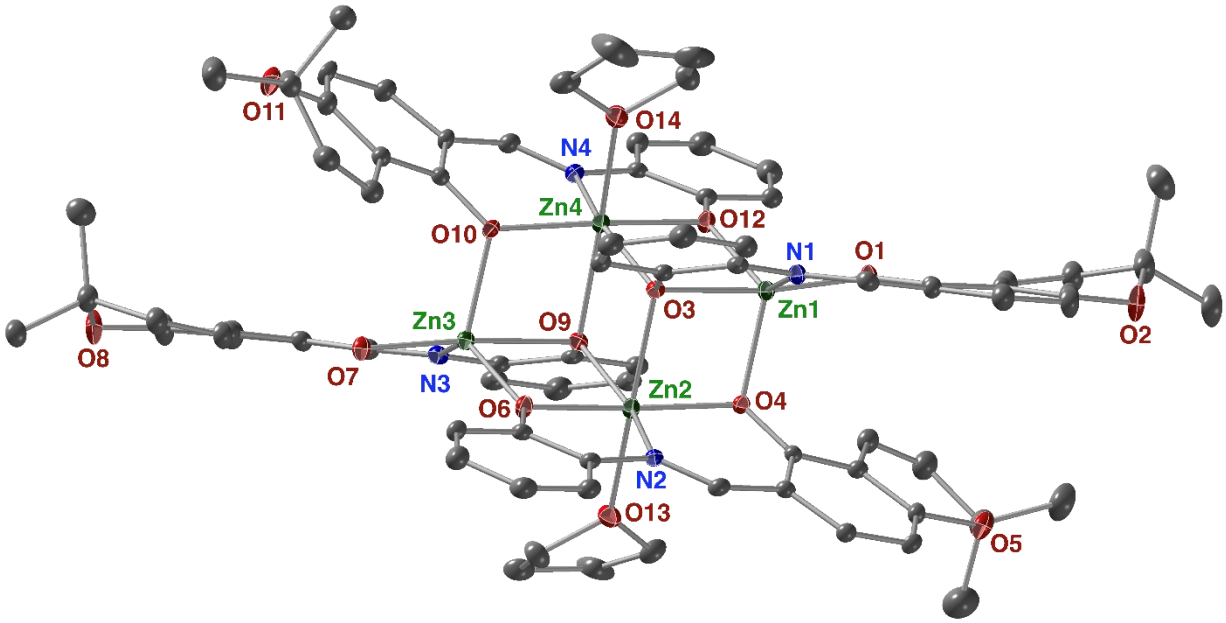

Fig. 1. Crystal structure of complex **3** $[Zn_4L_4(THF)_2]$ with ellipsoids drawn at 50% probability. Hydrogen atoms have been omitted for clarity.

The tetranuclear complex contains two types of zinc centers. Two Zn ions (Zn1 and Zn3) are 5-coordinate, each binding to three chromene ligands, while Zn2 and Zn4 are 6-coordinate, each binding to three chromene ligands and a molecule of THF solvent. The geometry of the 5-coordinate zinc centers can be described as distorted rectangular pyramidal with an average τ value of 0.47.[26] The defective dicubane core structure, Fig. 2, is visually symmetric to inversion but has enough structural asymmetry to preclude an inversion center. The 5-coordinate zinc centers have slightly longer Zn-O bonds when compared to the 6-coordinate zinc centers, with average Zn-O bond distances of 2.005(8) Å and 2.109(10) Å, respectively. Within the core, the Zn2-O3 and Zn4-O9 bonds average 2.268(4) Å, while the Zn4-O3 and Zn2-O9 bonds average 2.020(4) Å and the μ_3 Zn-O bonds average 2.194(7) Å while the μ_2, Zn-O bonds average 2.021(8) Å.

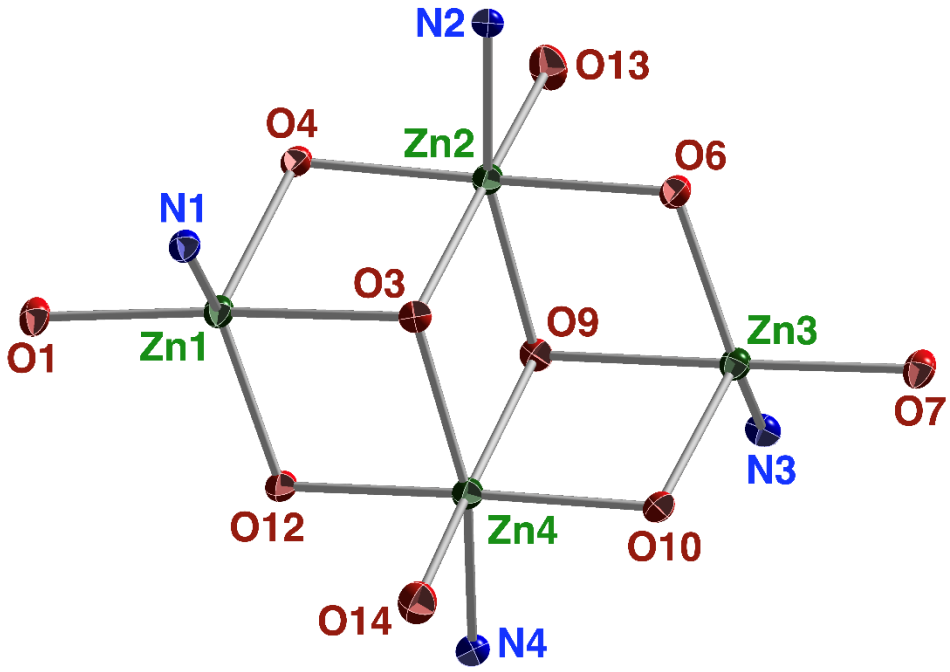

Fig. 2. Defective dicubane core of complex **3.** Selected bond lengths (Å): Zn1-O1: 1.943(3), Zn1-O3: 2.202(3), Zn1-O4: 2.068(3), Zn1-O12: 1.979(3), Zn2-O3: 2.267(3), Zn4-O3:2.038(3), Zn2-O13 (THF): 2.210(3).

2.2.2 Structure of $Ni_4L_4(THF)_2$, ***4***

Analysis of the X-ray diffraction data of the nickel complex, **4**, revealed a tetranuclear defective dicubane similar to the zinc complex, **3** (Fig. 3). However, there are some differences between the two complexes. The average metal-ligand bond lengths are shorter in the nickel derivative with average M-O distances of 2.037(13) Å for **4** and 2.076(13) Å for **3** and average M-N distances of 1.983(6) Å and 2.035(8) Å, respectively. The 5-coordinate nickel centers are also best described as distorted rectangular pyramids but have a lower average τ parameter of 0.42 suggesting the nickel centers are a bit closer to a true tetragonal geometry than their zinc counterparts. A similar defective dicubane formed from two [$NiNO_5$] and two [$NiNO_4$] moieties was previously reported by Nemec and coworkers,[16] with coordinated methanol solvent and a

biphenol Schiff-base ligand having similar average Ni-O and Ni-N bond distances to **4** at 2.045(6) and 1.966(5) Å, respectively. It should be noted that when complex **4** was prepared using a 2:1 ratio of $Ni(OAc)_4.4H_2O$: ligand **2**, the same complex was obtained as with the equimolar ratio.

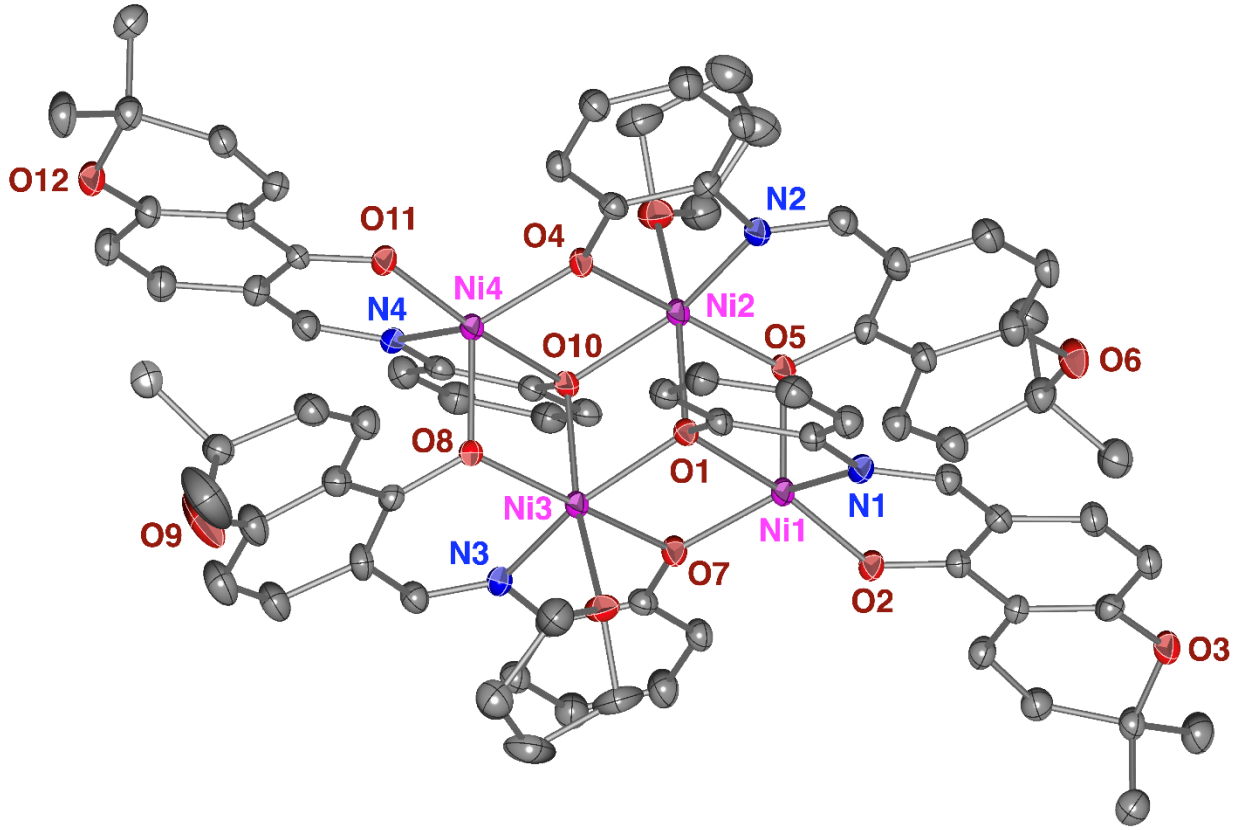

Fig. 3. Crystal structure of complex **4** $[Ni_4L_4(THF)_2]$ with ellipsoids drawn at 50% probability. Hydrogen atoms have been omitted for clarity.

*2.2.3 Structure of Fe_4L_6 (**5**)*

X-ray diffraction analysis of complex **5** confirmed the formation of a star-shaped tetranuclear Fe_4 cluster (Fig. 4) with a central FeO_6 unit and three radial FeO_4N_2 units joined to the center through μ_2-O bridges (Fig. 5). A star complex with identical coordination pattern to **5** was obtained by Dutta and Takahashi,[20-21] using a salicylaldehyde-derived iminophenolate ligand.

The complexes were generated in the presence of Fe(II) or Fe(III) metal salts. As noted by Takahashi, the central Fe(III) ion is bound to the ligand in a specific manner, i.e. it is coordinated only to the phenolate that originated from the aminophenol. For the other three iron ions, each is coordinated to two ligands through the imine nitrogen and the two phenolate ions originating from both the aminophenol and the chromene. One major difference between complex **5** and the previously reported structure is that **5** crystallized on a 2-fold rotation axis leading to half the molecule being symmetry equivalent, which was not the case in the salicylaldehyde derivative. Unlike **3** and **4**, where THF acts as a ligand, the THF solvent molecules are non-coordinated in **5**, packing in voids between the Fe_4L_6 complexes.

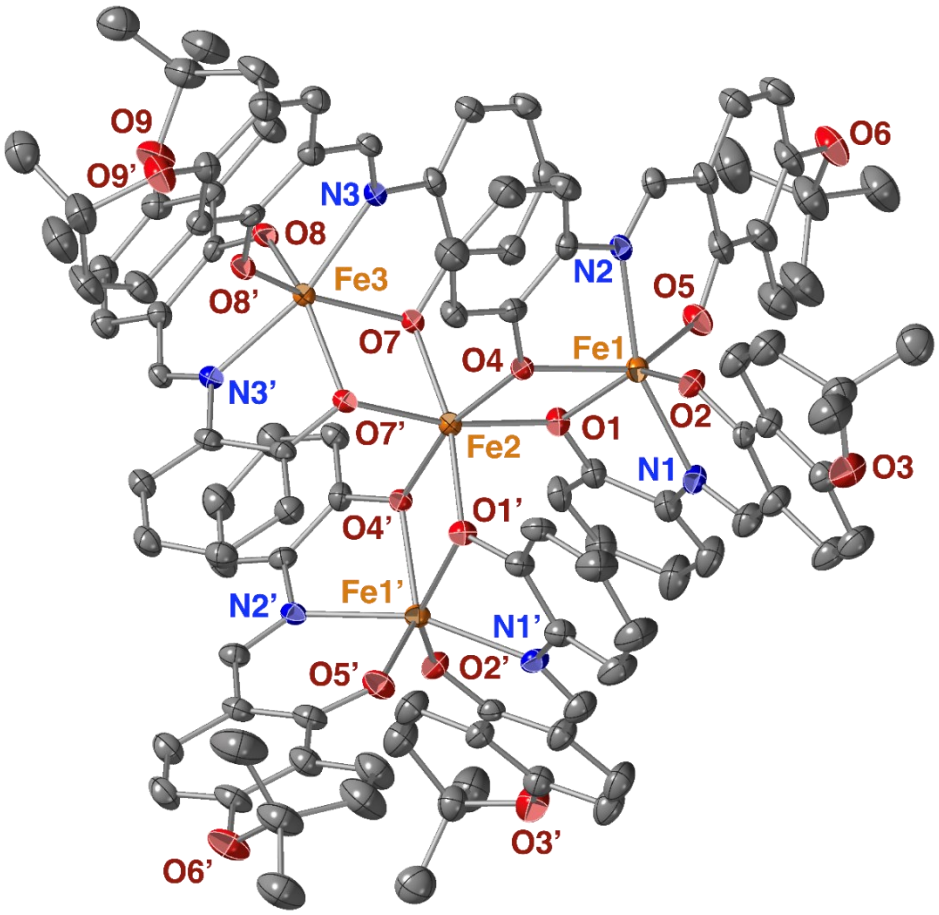

Fig. 4. Crystal structure of complex **5** [Fe_4L_6] with ellipsoids drawn at 50% probability. Hydrogen atoms have been omitted for clarity.

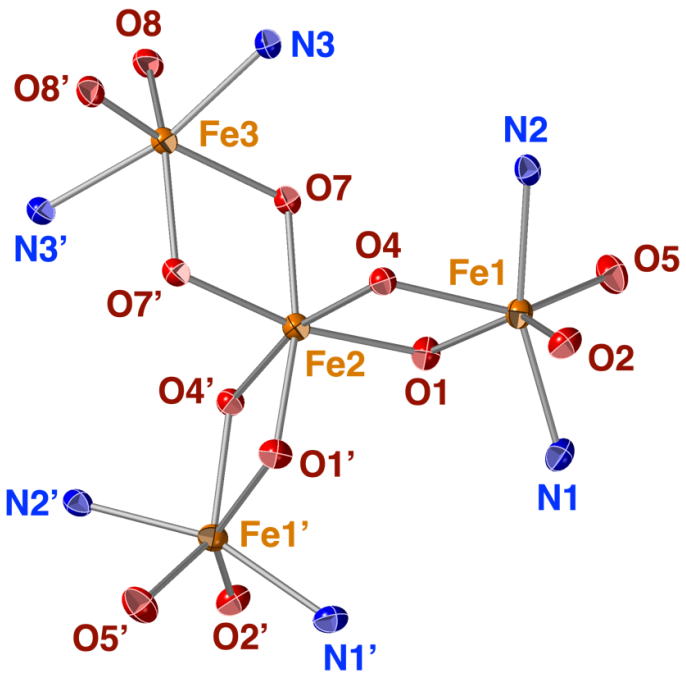

Fig. 5. Fe_4 star-shaped core of complex **5** with ellipsoids drawn at 50% probability. Selected bond lengths (Å): Fe1-O1: 2.067(3), Fe1-O4: 2.092(3), Fe2-O1: 1.977(3), Fe2-O4: 2.001(3), Fe2-O7: 2.007(3), Fe3-O7:2.068(3).

2.3. Mass Spectrometry Analysis of Chromene-Aminophenol Complexes (3-5)

X-ray diffraction investigates the solid-state structure of molecules but may not give definitive information about the species present in solution. The soft ionization used in ESI-MS has been shown to minimize fragmentation and provide insight into the solution-state composition of polymetallic clusters.[19,27] High resolution ESI-MS spectra were collected on complex **3** dissolved in a mixture of DMSO and methanol (Fig. S5 in supplementary data). The major peak, at 436.0567 *m/z*, corresponds to the mononuclear $[Zn(HL)(DMSO)]^+$. Traces of polymetallic clusters were also identified with barely-detectable peaks observed at 795.0887 *m/z*, corresponding to $[Zn_2(HL)L(DMSO)]^+$, and 1186.0888 *m/z*, corresponding to $[Zn_3(HL)L_2(DMSO)(MeOH)]^+$. No peak was observed for the tetranuclear complex in either

sample. These results indicate that the tetranuclear zinc complex dissociates mainly to a mononuclear species in coordinating solvents with a negligible amount of polymetallic clusters present in solution. This is quite different from the equilibrium of higher-nuclearity polymetallic species detected by ESI-MS for a similar Cu_4L_4 cubane-like complex.[27]

ESI-MS was also performed on the nickel and iron complexes under similar conditions (Figures S6 & S7). Similar to the zinc complex, the major metal-containing species in both complexes is a solvated mononuclear species with peaks observed at 430.0682 *m/z* corresponding to $[Ni(HL)(DMSO)]^+$ and 505.0583 *m/z* corresponding to $[FeL(DMSO)_2]^+$. However, there are some differences between the complexes. In the nickel derivative, the base peak is free ligand (296.1330 *m/z*, $[HL]^+$) and nothing larger than a bimetallic cluster was detected (703.0919 *m/z*, $[Ni_2(HL)L]^+$) in any real abundance. In the iron complex, only mononuclear species were detected at any real abundance with $[Fe(HL)_2(MeOH)_2]^+$ detected at 708.2288 *m/z*. These results suggest that the Fe star-shaped cluster may be more prone to dissociation in solution when compared to the defective dicubane structure found in both the nickel and zinc cases.

2.4. DNA cleavage studies of 2

The DNA cleavage ability of transition metal complexes has been well documented.[28-37] We anticipated that ligand **2** would catalyze DNA cleavage in the presence of highly redox-active metals ions such as Fe and Cu due to the increase in reactive oxygen species (ROS) during redox cycling in the presence of oxygen.[35,38] Attempts to prepare the Cu(II) complex of the chromene-aminophenol ligand did not produce crystals suitable for structural analysis.

Furthermore, mass spectrometric data for the $Zn_4L_4(THF)_2$ complex (**3**) suggested that the tetranuclear complex is not present in DMSO solution. Based on these two factors, pBR322 plasmid DNA cleavage was studied using *in situ*-generated complexes of (**2**) in the presence of various transition metal(II) acetate salts (Fe, Co, Ni, Cu, Zn and Cd). The extent of cleavage of supercoiled plasmid DNA (SC) to open circular (OC), linear (L) or fragmented forms in the presence of **2** (1 mM) and metal salts, or metal salts alone, was monitored by gel electrophoresis. As illustrated in Fig. 6, in the absence of ligand **2**, Fe(II) acetate (lane 1) caused cleavage of the DNA to predominantly the open-circular form compared to the control (lane 7). However, all the other metals ions (lanes 2-6) showed no cleavage activity. In the presence of ligand **2** (Fig. 7), both Fe(II) and Cu(II) acetate (lanes 1 and 4) showed cleavage of pBR322 while the other salts were ineffective. Based on the observation that the Fe(II) salt exhibits nuclease activity in the absence of **2**, no conclusions can be made regarding the effect of adding the ligand. However, these data suggest that complex formation is most likely responsible for the nuclease activity observed in the presence of Cu(II). These data are aligned with previous studies involving copper complexes of ligands that are similar to **2**.[28-29, 34-35]

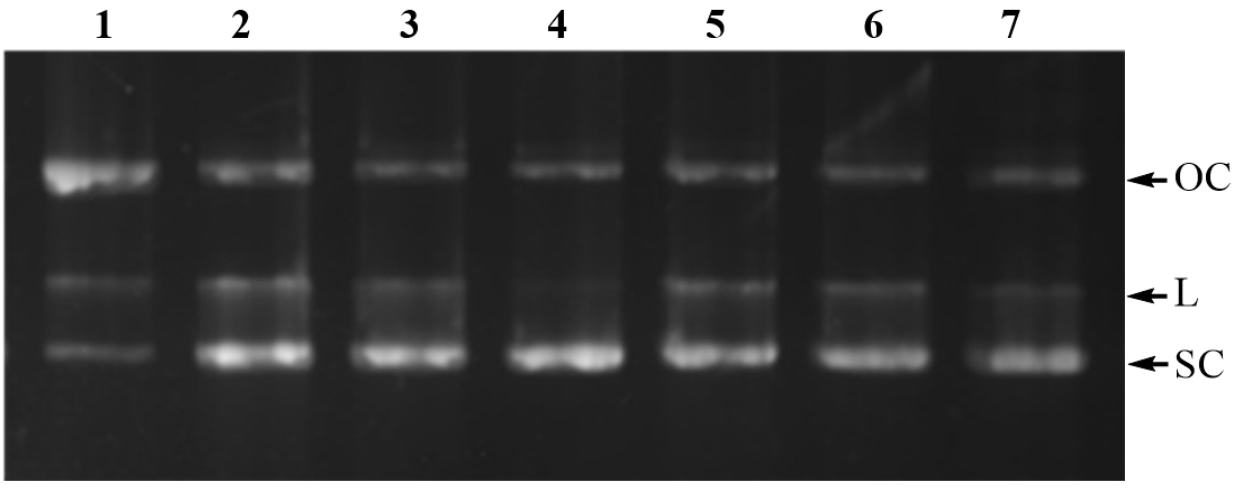

Fig. 6. DNA cleavage analysis in the presence of metal acetate salts. All lanes contain pBR322 DNA (0.25 μg) and the indicated metal salts at 1 mM. Lane 1: $Fe(OAc)_2$; Lane 2: $Co(OAc)_2$; Lane 3: $Ni(OAc)_2$; Lane 4: $Cu(OAc)_2$; Lane 5: $Zn(OAc)_2$; Lane 6: $Cd(OAc)_2$); Lane 7: DNA control. OC: open-circular; L: linear; SC: supercoiled.

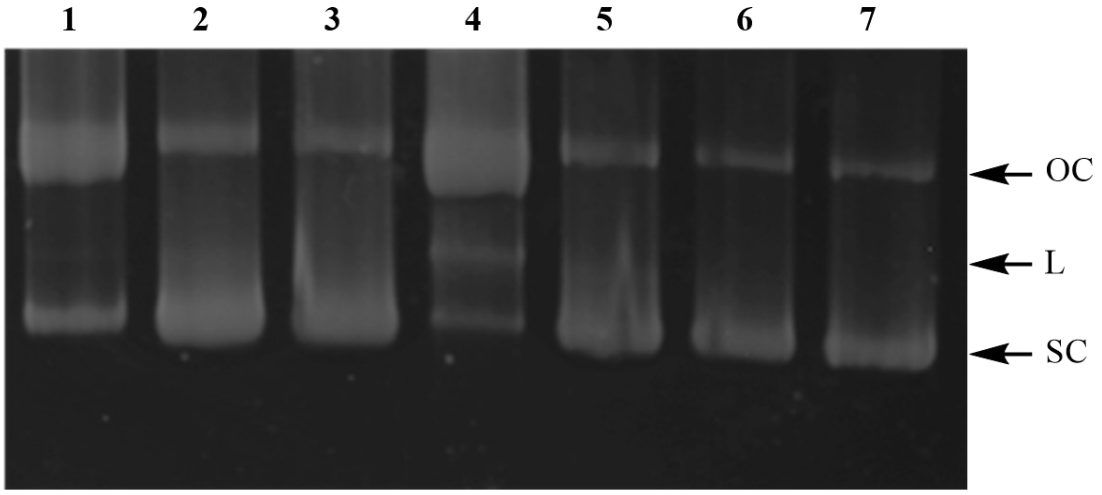

Fig. 7. DNA cleavage analysis of **2** (1.0 mM) in the presence of metal salts. Lanes 1-7 contain pBR322 DNA (0.25 μg) and the indicated compounds. Lane 1: **2** + Fe(II); Lane 2: **2** + Co(II); Lane 3: **2** + Ni(II); Lane 4: **2** + Cu(II); Lane 5: **2** + Zn(II); Lane 6: **2** + Cd(II); Lane 7: DNA control

In order to determine the possible mechanism of cleavage by ligand **2** in the presence of Cu(II) acetate, the cleavage experiment was conducted in the presence of hydroxyl radical (DMSO and *tert*-butanol), singlet oxygen (NaN_3 and histidine), and superoxide anion (KI and tiron) scavengers/quenchers (Fig. 8). Similar to Cu(II) acetate (lane 2), ligand **2** alone showed no significant cleavage of the DNA (lane 3) relative to the DNA control (lane 1). The addition of ROS scavengers/quenchers additives (lanes 5-10) did not significantly affect the copper-mediated cleavage ability of **2** (lane 4). These data suggest that reactive oxygen species do not play a major role in DNA cleavage, and the mechanism of DNA cleavage may be hydrolytic rather than oxidative.[36-37]

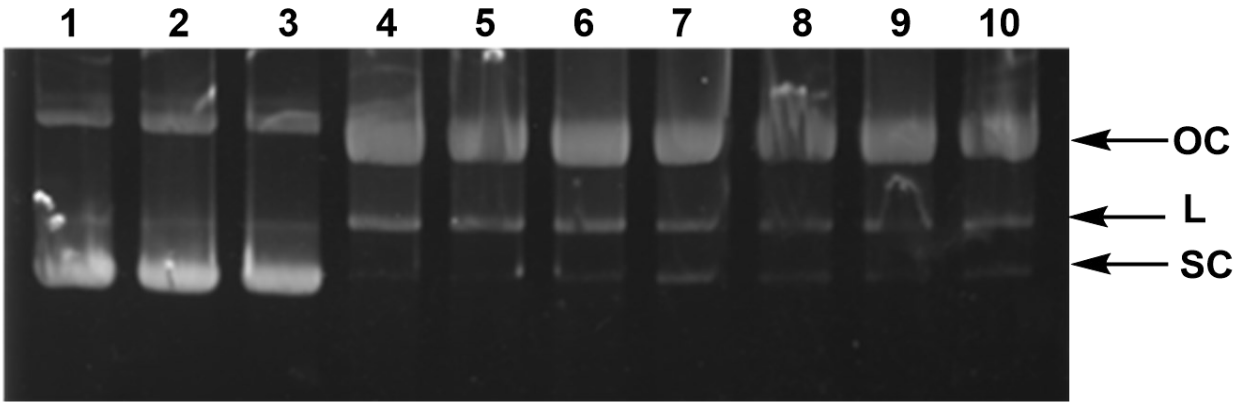

Fig. 8. The effect of ROS scavengers/quenchers on the cleavage of pBR322 DNA (0.25 μg) by **2** (500 μM) in the presence of copper acetate at 37°C for 1h. H_2L **2** (0.5 mM), scavengers and $Cu(OAc)_2$ (1.0 mM). *Lane 1*: DNA control; *Lane 2*: DNA + $Cu(OAc)_2$; *Lane 3*: DNA + **2**; *Lane 4*: DNA + **2** + $Cu(OAc)_2$; *Lane 5*: DNA + **2** + $Cu(OAc)_2$ + DMSO; *Lane 6*: DNA + **2** + $Cu(OAc)_2$ + *t*-BuOH; *Lane 7*: DNA + **2** + $Cu(OAc)_2$ + NaN_3; *Lane 8*: DNA + **2** + $Cu(OAc)_2$ + histidine; *Lane 9*: DNA + **2** + $Cu(OAc)_2$ + KI; *Lane 10*: DNA + **2** + $Cu(OAc)_2$ + tiron.

2.5 DNA binding studies of 2

The DNA absorption band at 260 nm represents $\pi \rightarrow \pi^*$ transitions of the purine and pyrimidine bases. Intercalation causes conformational changes in the DNA, leading to a hypochromic shift. In contrast, groove binding leads to damage and uncoiling of the DNA. As hydrogen bonding interactions between base pairs decrease upon helix uncoiling, the absorbance of the DNA bases increase, leading to a hyperchromic effect. [28,31-33,39-40]

The ability of ligand **2** to cleave DNA in the presence of Cu(II) ions suggests interaction with the DNA. To probe this interaction, a UV-Vis absorbance titration of calf-thymus DNA (CT-DNA, 89.4 μM) in the presence of increasing amounts of **2** (7.0-43 μM) was performed. As illustrated in Fig. 9, compound **2** exhibits concentration-dependent hyperchromism upon interaction with DNA, suggesting that **2** binds to the groove of DNA. The ability of salicylaldehyde and/or aminophenol-derived Schiff bases to act as groove binders or intercalators

is influenced by the nature of the substituents and other structural features. For example, similar to Schiff base **2**, a substituted salicylaldehyde-aminobenzoic acid ONO Schiff base ligand exhibited groove binding mode.[39] In contrast, a ONO Schiff base formed by condensation of 2-aminophenol and 5-chloro-2-hydroxybenzaldehyde displayed intercalative binding mode,[40] even though it is more structurally similar to **2** than the aminobenzoic acid derivative. The steric bulk of the dimethyl pyran ring in Schiff base ligand **2** potentially limits DNA intercalation.

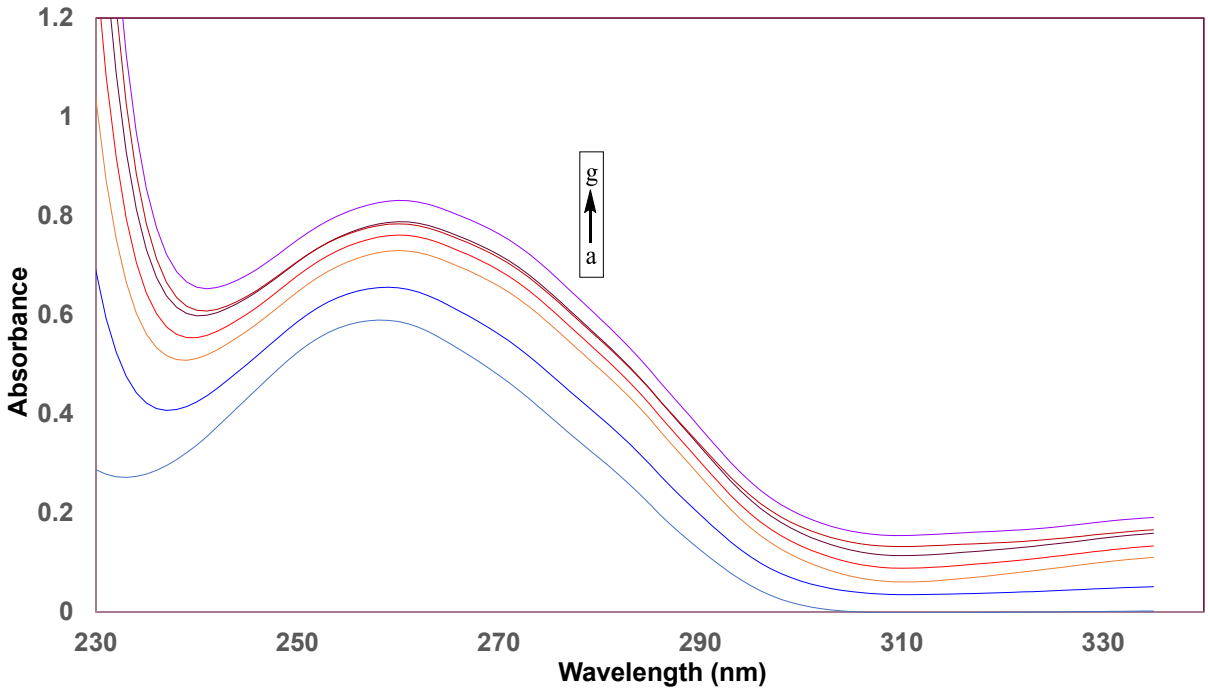

Fig. 9. UV-Vis absorption spectra of CT-DNA (89.4 μM) in the absence and presence of increasing amounts of **2** (7.0-43 μM) in Tris HCl buffer (50 mM, pH = 7.2). The arrow indicates absorbance changes at 260 nm with increase in the concentration of **2**. a) DNA + 0 μM **2**, b) DNA + 7.1 μM **2**, c) DNA + 14.1 μM **2**, d) DNA + 21.4 μM **2**, e) DNA + 28.6 μM **2**, f) DNA + 35.7 μM **2**, g) DNA + 42.9 μM **2**.

2.6 Molecular Docking Interactions of 2 with B-DNA

In order to further explore the interaction of H_2L (**2**) with DNA, molecular docking analysis was performed using Autodock Vina. Because of the observed dissociation of the zinc complex into monosolvated and disolvated monomeric complexes in DMSO, the docking affinities of H_2L, ZnL(DMSO) and $ZnL(DMSO)_2$ toward Dickerson-Drew B DNA dodecamer (PDB ID: 1BNA)[41] were compared. All three structures were found to dock at the minor groove (Fig. 10), supporting the data obtained from the UV-Vis binding studies. The free ligand H_2L displayed the highest docking affinity towards DNA, with a stabilization energy of -8.0 kcal/mol. This docking score is consistent with that of a ONO Schiff base with a similar mode of binding.[39] Generally, greater solvation was found to reduce the stabilization to -7.7 kcal/mol for ZnL(DMSO) and -6.2 kcal/mol for $ZnL(DMSO)_2$. The similar binding position of all three substrates suggests that H_2L facilitates the interaction of the metal with DNA by bringing them into close proximity through coordination.

The trend in docking affinity for H_2L, ZnL(DMSO) and $ZnL(DMSO)_2$ is further explained by the 2D interaction maps (Fig. 11). The ligand-DNA complex is stabilized primarily by hydrogen bonding interactions between the two phenol groups on H_2L and the deoxyribose oxygen atoms of guanine containing nucleotides on different chains, with the phenol groups functioning as hydrogen bond donors. For ZnL(DMSO), the oxygen that is part of the phenol on the chromene unit is hydrogen bonded to one guanine residue. However, no stabilizing hydrogen bonding interaction is observed between $ZnL(DMSO)_2$ and the DNA helix.

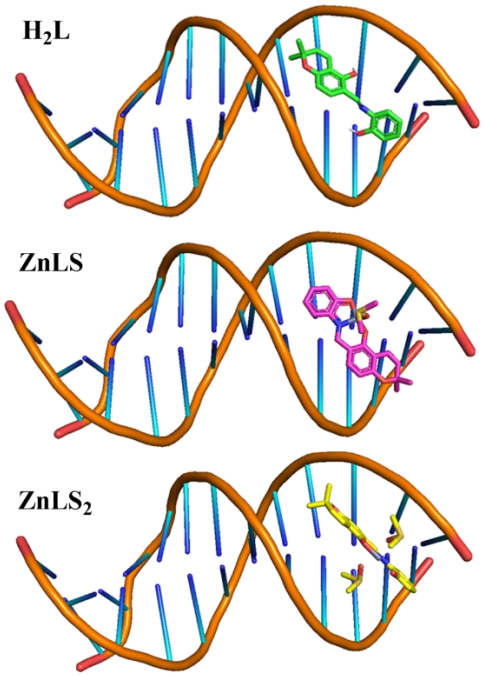

Fig. 10. Best docked structure of H_2L, ZnLS and $ZnLS_2$ in the minor grooves of the DNA dodecamer duplex of sequence d(CGCGAATTCGCG)2 (PDB ID: 1BNA) in Pymol. S = DMSO

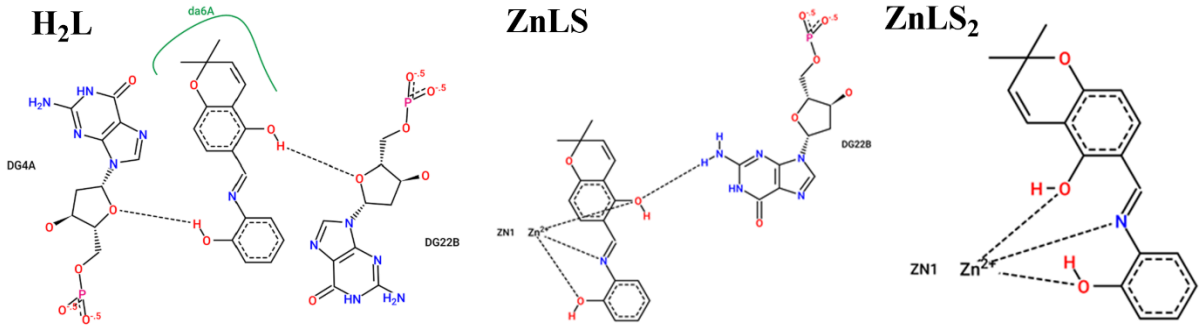

Fig. 11. ProteinsPlus 2D Interaction map of H_2L, ZnLS and $ZnLS_2$ with DNA. S = DMSO

3. Conclusions

Tetranuclear Zn(II), Ni(II) and Fe(III) complexes of a chromene-based Schiff-base ligand were synthesized and characterized by X-ray crystallography, and HRMS analysis. The Zn and Ni complexes were obtained as defective dicubane clusters, while the Fe complex was obtained as a star-shaped cluster, although the mononuclear complexes predominated in DMSO. Ligand

H_2L facilitated the Cu-mediated cleavage of plasmid DNA. UV-Vis spectroscopic binding studies and molecular docking analyses suggest that the ligand interacts with DNA by a groove binding mode.

4. Experimental section

4.1 Materials and Measurements

All reagents were obtained from commercial sources and used without further purification. pBR322 plasmid DNA was obtained from Fisher Scientific. Unless specified, reactions were performed open to air, and organic reactions were monitored by thin-layer chromatography (TLC) using silica gel plates, developed in 50% ethyl acetate/ hexanes. Plate visualization was performed under UV light (254 nm) and by staining with cerium-ammonium-molybdate (CAM) solution. NMR data (^{1}H, 400 MHz and ^{13}C, 100 MHz) were recorded on a JEOL 400 MHz instrument (Susquehanna University; NSF MRI: CHE-1625340) using $CDCl_3$ and DMSO-d_6 as solvents. High resolution ESI-MS data were acquired using a Waters SYNAPT G2-S QTOFMS system (University of Rhode Island) and an Agilent 6560 ion mobility Q-ToF mass spectrometer with Agilent Jet Spray dual ESI inlet (Bucknell University; NSF MRI: CHE-2018547). UV-Vis data were acquired on a Cary 4000 UV-Vis spectrometer. Agarose gels were visualized with Azure Biosystems c300 Western blot imager at 302 nm. Elemental analysis was performed by Atlantic Microlab, Inc., Norcross GA.

4.2 Synthetic Procedures

*4.2.1 Synthesis of Schiff base ligand, H_2L (**2**)*

The ligand H_2L [(*E*)-6-(((2-hydroxyphenyl)imino)methyl)-2,2-dimethyl-2*H*-chromen-5-ol] (**2**) was prepared by the condensation of 5-hydroxy-2,2-dimethyl-2H-chromene-6-carbaldehyde (**1**)[25] (500 mg, 2.44 mmol) and *ortho*-aminophenol (267 mg, 2.44 mmol) in absolute ethanol (27 mL) with a catalytic amount of acetic acid. After refluxing overnight, the reaction mixture was cooled, and the ethanol was removed in vacuo. The resulting orange solid was rinsed with water and dried to afford H_2L as an orange powder (711 mg, 99%). The product was determined to be pure by NMR spectroscopy and was used without further purification.

M.p.: 167-169 °C; IR (ATR), cm^{-1}: 1625, 1582, 1528, 1450, 1232, 1209, 1155, 1111. UV–Vis (DMSO: water, 7:3), λmax (nm): 435, 372.

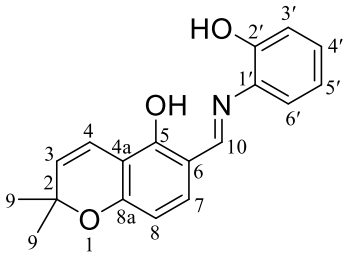

^{1}H NMR (DMSO-d_6) δ 15.06 (broad s, OH), 9.92 (broad s, OH), 8.80 (s, H-10), 7.39 (d, *J* = 8.0 Hz, H-6') 7.25 (d, *J* = 8.4 Hz, H-7), 7.06 (t, *J* = 8.0 Hz, H-4'), 6.92 (d, *J* = 8.0 Hz, H-3'), 6.85 (t, *J* = 8.0, H-5') 6.63 (d, *J* = 10.0, H-4), 6.23 (d, *J* = 8.4, H-8), 5.61 (d, *J* = 10.0, H-3), 1.36 (s, H-9). ^{13}C NMR (DMSO-d_6) δ 163.9 (C-10), 159.4 (C-5), 158.2 (C-8a), 150.5 (C-2'), 134.3 (C-7), 132.6 (C-1'), 127.9 (C-3, C-4'), 120.2 (C-5'), 119.0 (C-3'), 116.8 (C-4), 116.6 (C-4a), 113.1 (C-6'), 109.7 (C-6), 107.9 (C-8), 77.5 (C-2), 28.3 (C-9).

HRESI-MS *m/z*: calcd, for $C_{18}H_{18}NO_3$ 296.13; found 296.1296 ($M+H^+$).

*4.2.2 Preparation of H_2L Zinc complex (**3**)*

A warm solution of H_2L, **2** (61.5 mg, 0.208 mmol) in ethanol (6 mL) was added dropwise to a warm solution of $Zn(CH_3CO_2)_2{\cdot}2H_2O$ (45.9 mg, 0.209 mmol) in ethanol (4 mL), with stirring. A

yellow precipitate was formed as the addition continued. This mixture was refluxed for 1 hour before being cooled. Filtration of the resulting precipitate followed by rinsing with cold ethanol gave a yellow solid (53.9 mg). The solid was redissolved in a minimum amount of THF and the resulting yellow solution was filtered through Celite. The solvent was removed via rotary evaporation and the resulting solid dried under vacuum yielding a yellow solid (25.0 mg, 20% yield). Anal. Calcd: C, 60.85; H, 4.85; N, 3.55. Found: C, 61.0; H, 4.85; N, 3.49. Crystals suitable for X-ray diffraction were obtained from THF by slow diffusion of pentane.

*4.2.3 Preparation of H_2L Nickel complex (**4**)*

A warm solution of H_2L, **2** (62.0 mg, 0.210 mmol) in absolute ethanol (6 mL) was added to a warm solution of $Ni(CH_3CO_2)_2 \cdot 4H_2O$ (52.2 mg, 210 mmol) in ethanol (4 mL) and the mixture was heated under reflux for 1 hour. The mixture was filtered to collect a brown powder (48.5 mg) which was then redissolved in a minimum amount of THF. The resulting red solution was filtered through Celite and the solvent was removed via rotary evaporation. The resulting orange solid was dried under vacuum and collected (24.0 mg, 24% yield). Anal. Calcd: C, 61.9; H, 4.93; N, 3.61. Found: C, 62.2; H, 5.15; N, 3.45. Crystals suitable for X-ray diffraction were obtained from THF by slow diffusion of pentane.

*4.2.4 Preparation of H_2L Iron complex (**5**)*

A warm solution of H_2L, 2 (61.8 mg, 0.209 mmol) in absolute ethanol (6 mL) was added to a warm solution of $Fe(CH_3CO_2)_2$ (36.9 mg, 0.212 mmol) in warm ethanol (4 mL). The reddish brown solution was heated under reflux for 1 hour, and filtered to afford a dark-colored powder (45.5 mg). The solid was redissolved in a minimum amount of THF and the resulting solution was filtered through Celite. The solvent was removed via rotary evaporation and the resulting

solid dried under vacuum yielding a red-brown solid (14.0 mg). Elemental analysis data were inconclusive. Crystals suitable for X-ray diffraction were obtained from THF by slow diffusion of pentane.

4.3 X-Ray Diffraction Crystallography

Single crystals were selected and mounted on a low background MiTeGen loop using Paratone immersion oil and cooled to the data collection temperature with a stream of dry nitrogen gas. Data were collected on a Bruker D8 Venture diffractometer with 0.71073 Å Mo-Ka microfocus radiation and a Photon II detector. Unit cell parameters were obtained from 24 data frames, 0.5º ω, and complete data collection strategies were determined for each crystal using the APEX3 suite.[42] Full data sets were collected using 0.5° oscillations of ϕ and ω, and processed using SAINT.[43] Each data set was treated with SADABS[44] absorption corrections based on redundant multi-scan data. The structures were solved by intrinsic phasing (SHELXT) and refined by least squares methods on F^2 (SHELXL) within APEX3.[45-46] All non-hydrogen atoms were refined with anisotropic displacement parameters and all hydrogen atoms were treated as idealized contributions using riding models. Additional details of the data collections and refinements are provided in the Supplementary Information. Crystallographic data are available in CIF format through the Cambridge Crystallographic Data Centre, deposition numbers 2196040-2196042.

4.4 DNA cleavage studies

The cleavage reaction was carried out in 25 mM Tris–HCl (pH 7.2) buffer containing pBR322 plasmid DNA (1.0 μL, 0.25 μg), metal (II) acetate, [Fe, Co, Ni, Cu, Zn, Cd] (1.0 mM), and H_2L

(1.0 mM). The total volume of the assay mixture was 20 μL. Samples were incubated at 37 °C for 1 hour, after which the reaction was stopped by adding of 1× DNA loading dye (5.0 μL) in pH 8.0 TBE (Tris–borate–EDTA) buffer. Finally, all samples were loaded on 1% agarose gel in TBE, and electrophoresis was carried in TBE buffer (90V for 90 minutes). The gel was stained with GelRed for 15 minutes and visualized using an Azure Biosystems Western blot imager at 302 nm. For the mechanistic experiment a concentration of 0.5 mM was used for the ligand **2** and 1 mM for copper acetate and the ROS scavengers and quenchers. The samples were incubated for 1 h prior to performing gel electrophoresis.

4.5 UV-Vis spectroscopic binding studies

The stock solution of calf thymus (CT-DNA) was prepared by dissolving 13 mg of CT-DNA in 10 mL of Tris HCl buffer (50 mM, pH = 7.2). The solution was stirred at room temperature for 14 hours to achieve homogeneity. The UV-Vis absorbance ratio of CT-DNA solution at 260 nm and 280 nm (A_{260}/A_{280}) was 1.87, indicating that DNA is sufficiently free from protein.[47] The concentration of CT-DNA was calculated by UV-Vis absorbance at 260 nm with the extinction coefficient 6600 $M^{-1}cm^{-1}$. The stock solution of chromene aminophenol ligand was prepared in DMSO (5 mM). Absorbance titration experiments were performed in Tris HCl buffer at room temperature with a DNA concentration of 89.4 μM, and ligand **2** concentration ranging from 7.0 to 43 μM. The Tris-HCl buffer was used as blank control. The amount of DMSO in the working solution was limited to less than 1%. The test solutions were allowed to equilibrate for at least 5 min before reading the absorbance measurements.

4.6 DNA docking studies

The X-ray crystal structure of B-DNA (PDB ID: 1BNA) dodecamer d(CGCGAATTCGCG)$_2$ was obtained from the Protein Data Bank (http://www.rcsb.org/pdb). Polar hydrogens were added and Kollman charges were assigned to the DNA prior to carrying out docking studies. The free chromene-aminophenol ligand, H_2L, and solvated ligands, ZnL(DMSO) and ZnL(DMSO)$_2$, were generated in Avogadro and subjected to energy optimization using a steepest-descent algorithm. Polar hydrogens were added using Open Babel software, prior to conversion to pdbqt files. Docking analyses were performed using AutoDock Tools version 1.5.6 and AutoDock Vina programs.[48] The grid box included the entire B-DNA structure, and nine conformational images were created for each ligand. The output files for the lowest energy conformers were exported to PyMol for display of the 3D structure of the DNA-aminophenol ligand complex. The 2D interaction diagrams were obtained using ProteinsPlus server.

Declaration of Competing Interest

The authors declare that they have no known competing financial interests or personal relationships that could have appeared to influence the work reported in this paper.

Acknowledgments

The authors are thankful to Susquehanna University for funding this work. We are also grateful to Dr. Lou Ann Tom (Susquehanna University) and Dr. Douglas Collins (Bucknell University) for assistance in acquiring high resolution mass spectrometry data.

Appendix A. Supplementary data

^{1}H NMR, ^{13}C NMR, and IR spectra of compound **2** are available in the supplementary file, together with additional crystallographic data for complexes **3-5**.

References

1. J. Kumar, A. Rai, V. Raj. A comprehensive review on the pharmacological activity of Schiff base containing derivatives. Org. Med. Chem. 1 (2017) 555564.

2. M.N. Uddin, S.S. Ahmed, S.M.R. Alam. REVIEW: Biomedical applications of Schiff base metal complexes. J. Coord. Chem. 73 (2020) 3109-3149.

3. A. Aragón-Muriel, V. Reyes-Márquez, F. Cañavera-Buelvas, J.R. Parra-Unda, F. Cuenú-Cabezas, D. Polo-Cerón, R. Colorado-Peralta, G.V. Suárez-Moreno, B.A. Aguilar-Castillo, D. Morales-Morales. Pincer complexes derived from tridentate Schiff bases for their use as antimicrobial metallopharmaceuticals. Inorganics. 10 (2022) 134.

4. D. Huang, X. Liu, S. Zhao, Z. Yang. Crystal structures of three transition metal complexes with salicylaldehyde-4-hydroxy phenylacetyl acylhydrazone and their interactions with CT-DNA and BSA. Polyhedron. 211 (2022) 115516.

5. J. Szklarzewicz, A. Jurowska, M. Hodorowicz, G. Kazek, M. Głuch-Lutwin, J. Sapa, M. Papież. Tridentate ONO ligands in vanadium(III-V) complexes - synthesis, characterization and biological activity. J. Mol. Struct. 1224 (2021) 129205.

6. G. Ayyannan, M. Mohanraj, M. Gopiraman, R. Uthayamalar, G. Raja, N. Bhuvanesh, R. Nandhakumar, C. Jayabalakrishnan. New palladium(II) complexes with ONO chelated hydrazone ligand: Synthesis, characterization, DNA/BSA interaction, antioxidant and cytotoxicity. Inorganica Chim. Acta 512 (2020) 119868.

7. İ. Gönül. Synthesis and structural characterization of ONO type tridentate ligands and their Co(II) and Ni(II) complexes: Investigation of electrical conductivity and antioxidant properties. Inorganica Chim. Acta. 495 (2019) 119027.
8. Y. Burgos-Lopez, J. Del Plá, L.M. Balsa, I.E. León, G.A. Echeverría, O.E. Piro, J. García-Tojal, R. Pis-Diez, A.C. González-Baró, B.S. Parajón-Costa. Synthesis, crystal structure and cytotoxicity assays of a copper(II) nitrate complex with a tridentate ONO acylhydrazone ligand. Spectroscopic and theoretical studies of the complex and its ligands. Inorganica Chim. Acta. 487 (2019) 31-40.
9. D. Rogolino, M. Carcelli, A. Bacchi, C. Compari, L. Contardi, E. Fisicaro, A. Gatti, M. Sechi, A. Stevaert, L. Naesens. A versatile salicyl hydrazonic ligand and its metal complexes as antiviral agents. J. Inorg. Biochem. 150 (2015) 9-17.
10. B.K. Muñoz, M. Viciano, C. Godard, S. Castillón, M. García-Ruiz, M.D.B. González, C. Claver. Metals bearing ONO ligands as highly active catalysts in carbon dioxide and epoxide coupling reactions. Inorganica Chim. Acta. 517 (2020) 120194.
11. I. Mylonas-Margaritis, P.S. Perlepe, M. Masič, C.P. Raptopoulou, V. Psycharis, A. Escuer, S.P. Perlepes . Carbonato- and methanediolato(-2)-bridged nickel(II) coordination clusters from the use of N-salicylidene-4-methyl-o-aminophenol. *Inorg. Chem. Commun*. 83 (2017) 113-117.
12. M.M. Belmonte, E.C. Escudero-Adán, E. Martin, A.W. Kleij. Isolation and characterization of unusual multinuclear Schiff base complexes: rearrangements reactions and octanuclear cluster formation. Dalton Trans. 41 (2012) 5193-5200.
13. N.E. Borisova, A. Kostin, T.V. Magdesieva, M.D. Reshetova, O. Nikitin, V. Paredes-García, M. T. Garland, P. Hermosilla-Ilbánez, W. Canon-Sancisidor, A. Rodionov, D.

Venegas-Yazigi, E. Spodine. Solvent switchable nuclearity of Cu^{II} complexes with 2,6-bis-((acetylamino)phenylimino)methyl)-4-*tert*-butylphenol (H_3L) ligand. New J. Chem. 38 (2014) 709-716.

14. S. Meghdadi, V. Mirkhani, K. Mereiter. Electrochemical synthesis and crystal structure studies of defective dicubane tetranuclear hydroxo and varboxiamide ligand bridged cobalt(II)-cobalt(III) complexes with varboxamides produced from unprotected hydroxaromatic carboxylic acids. C. R. Chimie 18 (2015) 654-661.
15. J. Mayans, A. Martin, M. Font-Bardia, A. Escuer. Chiral tetranuclear NiII clusters derived from Schiff bases and azido co-ligands. Polyhedron 150 (2018) 10-14.
16. I. Nemec, R. Herchel, M. Machata, Z. Trávníček. Tetranuclear Ni(II) and Co(II) Schiff-base complexes with an M_4O_6 defective dicubane-like core: zero-field SMM behavior in the cobalt analogue. New J. Chem. 41 (2017) 11258.
17. R. Herschel, I. Nemec, M. Machata, Z. Trávníček. Solvent-induced structural diversity in tetranuclear Ni(II) Schiff-base complexes; the first Ni_4 single-molecule magnet with a defective dicubane-like topology. Dalton Trans. 46 (2016) 18622-18634.
18. L. Jiang, D. Zhang, J. Suo, W. Gu, J. Tian, X. Lui, S. Yan. Synthesis, magnetism and spectral studies of six defective dicubane tetranuclear $\{M_4O_6\}$ ($M = Ni^{II}$, Co^{II}, Zn^{II}) and three trinuclear Cd^{II} complexes with polydentate Schiff base ligands. Dalton Trans. 25 (2016) 10233-10248.
19. K. Griffiths, P. Kumar, G.R. Akien, N.F. Chilton, A. Abdul-Sada, G.J. Tizzard, G. S.J. Coles, G.E. Kostakis. Tetranuclear Zn/4f coordination clusters as highly efficient catalysts for Friedel-Crafts alkylation. Chem. Commun. 52 (2016) 7866-7869.

20. A.K. Dutta, S. Biswas, S. Dutta, L.N. Dawe, C.R. Lucas, B. Adhikary. Syntheses, structural, spectroscopic and magnetic properties of polynuclear Fe(III) complexes containing N and O donor ligands. Inorganica Chim. Acta 444 (2016) 141-149.
21. K. Takahashi, K. Kawamukai, T. Mochida, T. Sakurai, H. Ohta, T. Yamamoto, Y. Einaga, H. Mori, Y. Shimura, T. Sakakibara, T. Fujisawa, A. Yamaguchi, A. Sumiyama. Antiferromagnetic Transition in a Novel Star-shaped High-spin Fe(III) Tetranuclear Cluster from a Mononuclear Coordination Anion Featuring π-Extended Schiff Base Ligands. Chem. Lett. 44 (2015) 840-842.
22. S. Mondal, S. Mandal, A. Jana, S. Mohanta. Dinuclear, star-shaped tetranuclear and trinuclear-based two-dimensional metal complexes derived from a less investigated Schiff base ligand: Syntheses, crystal structures and spectroscopic correlation. Inorganica Chim. Acta. 415 (2014) 138-145.
23. S. Khanra, K. Kuepper, T. Weyhermüller, M. Prinz, M. Raekers, S. Voget, A.V. Postnikov, F.M.F. de Groot, S.J. George, M. Coldea, M. Neumann, P. Chaudhuri. Star-shaped molecule of $Mn^{II}_4O_6$ Core with an $S_t = 10$ High-Spin State. A Theoretical and experimental study with XPS, XMCD, and other magnetic methods. Inorg. Chem. 47 (2008) 4607-4617.
24. M. Prinz, K. Kuepper, C. Taubitz, M. Raekers, S. Khanra, B. Biswas, T. Weyhermüller, M. Uhlarz, J. Wosnitza, J. Schnack, A.V. Postnikov, C. Schröder, S.J. George, M. Neumann, P. Chaudhuri. A star-shaped heteronuclear $Cr^{III}Mn^{II}_3$ species and its precise electronic and magnetic structure: Spin frustration studied by X-ray spectroscopic, magnetic, and theoretical methods. Inorg. Chem. 49 (2010) 2093-2102.

25. G.E. Henry, H. Jacobs. A short synthesis of 5-methoxy-2,2-dimethyl-2*H*-1-benzopyran-6-propanoic acid methyl ester. Tetrahedron. 57 (2001) 5335-5338.

26. W. Addison, T.N. Rao, J. Reedijk, J. van Rijn, G.C. Verschoor. Synthesis, structure, and spectroscopic properties of copper(II) compounds containing nitrogen–sulphur donor ligands; the crystal and molecular structure of aqua[1,7-bis(*N*-methylbenzimidazol-2′-yl)-2,6-dithiaheptane]copper(II) perchlorate. J. Chem. Soc. Dalton Trans. 7 (1984) 1349.

27. O.V. Nesterova, O.E. Bondarenko, A.L. Pombeiro, D.S. Nesterov. Phenoxazinone synthase-like catalytic activity of novel mono- and tetranuclear copper(II) complexes with 2-benzylaminoethanol. Dalton Trans. 49 (2020) 4710-4724.

28. K. Bengi, S. Maddikayala, S.R. Pulimamidi. DNA binding, cleavage, docking, biological and kinetic studies of Cr(III), Fe(III), Co(II) and Cu(II) complexes with ortho-vanillin Schiff base derivative. Appl. Organomet. Chem. 36 (2022) e6451.

29. M. Sumi, N.T. Nevaditha, B.S. Kumari. Synthesis, structural evaluation, antioxidant, DNA cleavage, anticancer activities and molecular docking study of metal complexes of 2-amino thiophene derivative. J. Mol. Struct. 1272 (2023) 134091.

30. S. Khursheed, S. Tabassum, F. Arjmand. Comprehensive biological {DNA/RNA binding profile, cleavage & cytotoxicity activity} of structurally well-characterized chromone-appended Cu(II)(L1-3)(phen) potential anticancer drug candidates. Polyhedron 214 (2022) 115638.

31. M.R. Rodríguez, M.J. Lavecchia, B.S. Parajón-Costa, A.C. González-Baró, M. R. González-Baró, E.R. Cattáneo. DNA cleavage mechanism by metal complexes of Cu(II), Zn(II) and VO(IV) with a Schiff-base ligand. Biochimie. 186 (2021) 43-50.

32. N.M. Abdul Khader Jailania, A. Xavierb, A. Ram. Synthesis, spectroscopic characterization, DNA binding ability and biological activities of transition metal complexes containing tridentate Schiff base. Mater. Today: Proc. 5 (2018) 22200-22214.
33. S. Tabassum, M. Afzal, H. Al–Lohedan, M. Zaki, R.A. Khan, M. Ahmad. Synthesis and structure elucidation of new open cubane tetranuclear [CuII4] cluster: Evaluation of the DNA/HSA interaction and pBR322 DNA cleavage pathway and cytotoxicity. Inorganica Chim. Acta. 463 (2017) 142-155.
34. Z. Chen, J. Zhang, S. Zhang. Oxidative DNA cleavage promoted by two phenolate-bridged binuclear copper(II) complexes. New J. Chem. 39 (2015) 1814-1821.
35. S. Tabassum, S. Amir, F. Arjmand, C. Pettinari, F. Marchetti, N. Masciocchi, G. Lupidi, R. Pettinari. Mixed-ligand Cu(II)-vanillin Schiff base complexes; effect of coligands on their DNA binding, DNA cleavage, SOD mimetic and anticancer activity. Eur. J. Med. Chem. 60 (2013) 216-232.
36. C. Liu, L, Wang. DNA hydrolytic cleavage catalyzed by synthetic multinuclear metallonucleases. Dalton Trans. (2009) 227-239.
37. C. Liu, M. Wang, T. Zhang, H. Sun. DNA hydrolysis promoted by di- and multi-nuclear metal complexes. Coord. Chem. Rev. 248 (2004) 147-168.
38. K.E. Prosser, S.W. Chang, F. Saraci, P.H. Le, C.J. Walsby. Anticancer copper pyridine benzimidazole complexes: ROS generation, biomolecule interactions, and cytotoxicity. J. Inorg. Biochem. 167 (2017) 89-99.
39. H.P. Gogoi, A. Singh, P. Barman, D. Choudhury. A new potential ONO Schiff-base ligand and its Cu(II), Zn(II) and Cd(II) complexes: Synthesis, structural elucidation, theoretical and bioactivity studies. Inorg. Chem. Commun. 146 (2022) 110153.

40. K.S. Munawar, S. Ali, S. Muhammad, M. Ashfaq, S.M. Abbas, M.N. Tahir, S.M. Siddeeg, G. Ahmed. Synthesis, crystal structure, Hirshfeld surface analysis, DNA binding, optical and nonlinear optical properties of Schiff bases derived from o-aminophenol. J. Mol. Struct. 1274 (2023) 134427.
41. S. Neidle. Beyond the double helix: DNA structural diversity and the PDB. J. Biol. Chem. 296 (2021) 100553.
42. APEX3, v. 2017.3; Bruker AXS Inc.: Madison, WI, 2017.
43. SAINT, v. 8.38a; Bruker AXS Inc.: Madison, WI, 2016.
44. SADABS, v. 2016/2; Bruker AXS Inc: Madison, WI, 2016.
45. G.M. Sheldrick. Crystal structure refinement with SHELXL. Acta Crystallogr. C71 (2015) 3-8.
46. G.M. Sheldrick, SHELXT-Integrated space-group and crystal-structure determination. Acta Crystallogr. A71 (2015) 3-8.
47. D.B.M.A. van Wieren-de Weijer, A.H. Maitland-van der Zee, A. de Boer, S.V. Belitser, A.A. Kroon, P.W. de Leeuw, P. Schiffers, R.G. Janssen, C.M. van Deijn, B.H.C.H. Stricker, O.H. Klungel. Determinants of DNA yield and purity collected with buccal cell samples. Eur. J. Epidemiol. 24 (2009) 677-682.
48. O. Trott, A.J. Olson. AutoDock Vina: improving the speed and accuracy of docking with a new scoring function, efficient optimization and multithreading. J. Comput. Chem. 31 (2010) 455-461.